Front. Optoelectron. 2015, 8(2): 203–211
DOI 10.1007/s12200-015-0516-9

RESEARCH ARTICLE

Effect of light beam on measurements of reflectance and transmittance of turbid media with integrating sphere: Monte Carlo simulation

Xiewei ZHONG, Shenxia TAN, Xiang WEN, Dan ZHU (✉)

Britton Chance Center for Biomedical Photonics, Wuhan National Laboratory for Optoelectronics, Huazhong University of Science and Technology, Wuhan 430074, China
Ministry of Education (MoE) Key Laboratory for Biomedical Photonics, Department of Biomedical Engineering, Huazhong University of Science and Technology, Wuhan 430074, China

Abstract Integrating sphere technique is widely used to measure the total reflectance and transmittance of turbid sample, but the unavoidable light loss induces some measuring error. It has never been reported whether the error depends on the shape and size of light beam. In this paper, a convolution for computing the responses to rectangular incident light beam based on the Monte Carlo method was presented. The effects of light beam shape and size, and optical properties of sample on the measurements were addressed. The results show that the light loss with rectangular incident light beam is larger than that with circular one with the same area. The more the area of light beam, the more the light loss. And the light loss induced by the optical properties of sample is much more significant than that by the shape and size of the incident light beam.

Keywords integrating spheres, optical properties, Monte Carlo

1 Introduction

Reflectance (R) and transmittance (T) are two very important parameters to evaluate optical property of material, such as leaf [1], intralipid [2,3] and tissues [4–15]. To measure the R and T accurately, the integrating sphere technique has been used due to all of the light reflected or transmitted in various directions can be collected with it. But unavoidably, in the measurements, some scattering radiation still escapes through the sides of the sample and the ports of sphere, which can introduce some error to the measurements [16].

Received February 11, 2015; accepted March 24, 2015

E-mail: dawnzh@mail.hust.edu.cn

To reduce the error in the measurements, previous researchers have studied the relationship between the light loss and different parameters, such as, the size of integrating-sphere port, the optical properties (absorption property and scattering property) of turbid media and the ratio of the sample diameter to light beam diameter. Zhu et al. demonstrated that the light loss could be reduced by enhancing the sample port diameter of the integrating sphere, decreasing the thickness of the sample, or increasing the absorption coefficient of the sample, but the error caused by the size of light beam has not been mentioned [16]. Pickering et al. indicated that large ratio of sample diameter to beam diameter could effectively reduce the light loss through the side of the sample, such as a 25-mm aperture for a 1-mm diameter beam [17].

However, for the spectroscopy systems with broadband light sources, the sample diameter may not exceed significantly the diameter of the incident beam, so the effect of the light beam size on the light loss in the R and T measurement should be further investigated. What's more, in the practical applications, the rectangular shape of light beam is used for the commercial spectrophotometers Lambda 900/950 (PerkinElmer, USA) and Cary 500/5000 (Varian, USA), which has been widely used for measuring R or T [15,18–21]. Up till now, there are few investigations to evaluate the effects of the rectangular incident beam on the R and T measurements, or to demonstrate the differences between the effects of the rectangular incident beam and the circular or pencil incident light beam.

Thus, in this paper, a convolution method based on the Monte Carlo simulation was presented to obtain the R and T with rectangular light beam incident on turbid sample. The losses of light with various incident light beams (rectangular, circular and pencil light beams) were

compared. In addition, the effects of optical properties and the rectangular incident light beam size on the light loss were also investigated.

2 Method

2.1 Light beam and light entrance ports

In this paper, the shape of the light entrances for the R and T simulation were all based on a commercially available spectrophotometer (Lambda 950, PerkinElmer, USA). Figure 1 shows the system diagram for spetrophotometer, and the typical geometric dimensions of integrating sphere entrances for R and T measurements were also given. The R-entrance is a circle (r = 1.270 cm); the T-entrance is combined two semi-circle (r = 0.811 cm) and one rectangular (weight × height = 1.622 cm × 0.778 cm). The gray-filled rectangle was the area of the incident light. The rectangular incident light area was controlled by setting the size of the beam slit and the common beam mask in Lambda 950. And then the (weight, height) of the incident light at the R and T entrance was measured manually.

2.2 Principle of convolution for the rectangular incident light beam

This section presented the principle and numerical computation of the convolution for rectangular light beam incident on turbid sample, based on the Monte Carlo simulation results of pencil incident light beam [22]. According to the implements of the convolution for the circular incident light beam [23], the responses to rectangular light beam can be obtained through the convolution:

$$\phi(x,y) = \int_0^{\infty} G(r')r' \left(\int_0^{2\pi} S\left(\sqrt{x^2 + y^2 + r'^2 - 2\sqrt{x^2 + y^2}r'\cos\theta'} \right) \mathrm{d}\theta' \right) \mathrm{d}r' . \quad (1)$$

Here, in order to implement the convolution easily, the cylindrical coordinate system was chosen. $S(r')$ denotes the intensity profile of the rectangular light beam, $G(r')$ represents the distribution of R or T with pencil light beam incident on turbid sample, r means the distance between the center of the rectangular incident light beam and the distribution point.

Figure 2 shows the diagram for how to convolute the responses to pencil light beam for obtaining the responses to the rectangular incident light beam. The red rectangular area represents the rectangular incident light beam and the colorful circle indicates the distribution of R or T with pencil incident light beam.

The θ' in Eq. (1) stands for the central angle, which is subtended by the arc (as indicated by arrow in Fig. 2) with the fixed r'. To simplify the double integral, Eq. (1) can be separated into two steps:

$$\begin{cases} s(r,r') = \int_0^{2\pi} S(\sqrt{r^2 + r'^2 - 2rr'\cos\theta'})\mathrm{d}\theta', \\ \phi(r) = \int_0^{\infty} G(r')r's(r,r')\mathrm{d}r', \end{cases}$$

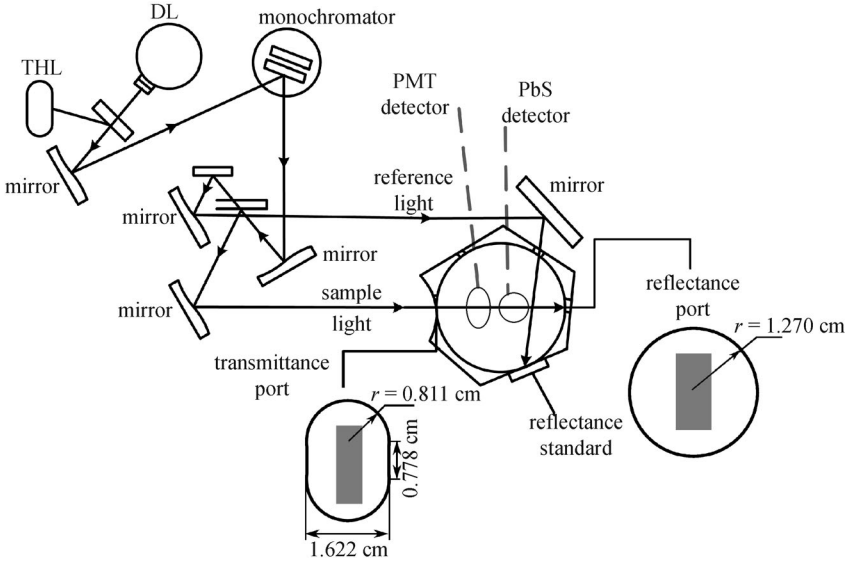

Fig. 1 System diagram for spectrophotometer and single integrating sphere. The geometry of the entrances for the R and T was also given. The gray-filled rectangle was the area of the incident light. THL: tungsten-halogen light source; DL: deuterium light source; PMT: photomultiplier

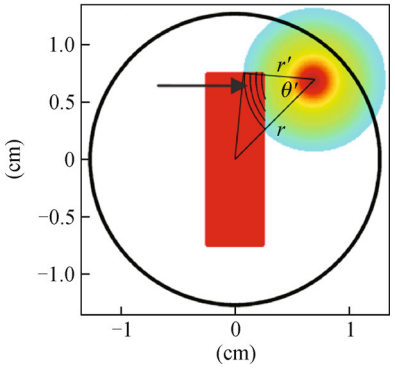

Fig. 2 Diagram for how to convolute with rectangular incident light beam. The red rectangular represents the rectangular incident light beam. The colorful circle indicates the reflectance with pencil incident light beam. The arrow shows the arc intersected by the light beam and the responses of the pencil light beam. The black circle indicates the port of integrating sphere

$$r = \sqrt{x^2 + y^2}. \tag{2}$$

2.3 Data analysis

The R and T were obtained with rectangular, circular and pencil light beam incident on turbid media, respectively. For modeling the R and T, some assumptions were listed in Table 1.

Here, the anisotropy, g, of the samples was assumed as 0.7, due to the g of intralipid, which was widely used in tissue phantoms, was about 0.7 [2]. In addition, the area of the circular incident light beam is equal to the rectangular light beam for suitable comparing.

After modeling the R and T with different geometries of incident light beam, the light losses with the rectangular, circular and pencil incident light beam in theory were calculated by below equations:

$$\delta_{\mathrm{R\_Geometry}} = \frac{R_{\mathrm{Total}} - R_{\mathrm{Geometry}}}{R_{\mathrm{Total}}}, \tag{3}$$

$$\delta_{\mathrm{T\_Geometry}} = \frac{T_{\mathrm{Total}} - T_{\mathrm{Geometry}}}{T_{\mathrm{Total}}}. \tag{4}$$

Here, R_{Total} and T_{Total} represent the total R and T of turbid media respectively. R_{Geometry} and T_{Geometry} represent R and T collected by integrating sphere with various incident light beams. And the subscript "Geometry" denotes "Rectangular," "Circular" and "Pencil," respectively.

The difference of the light loss between the responses to the rectangular incident light beam and other beams (circular and pencil) was calculated:

$$\Delta R_{\mathrm{Rect\_Geometry}} = \delta_{\mathrm{R\_Rectangular}} - \delta_{\mathrm{R\_Geometry}}, \tag{5}$$

$$\Delta T_{\mathrm{Rect\_Geometry}} = \delta_{\mathrm{T\_Rectangular}} - \delta_{\mathrm{T\_Geometry}}. \tag{6}$$

Here, the subscript "Geometry" represents "Circular" and "Pencil," respectively.

In addition, to evaluate the effect of rectangular light beam size on the light loss, the difference of the light loss between the responses to the light beams with various areas was obtained by below equations:

$$\Delta R_{\mathrm{Rect}} = \delta_{\mathrm{R\_Rect}(w,h)} - \delta_{\mathrm{R\_Rect}(w',h')}, \tag{7}$$

$$\Delta T_{\mathrm{Rect}} = \delta_{\mathrm{T\_Rect}(w,h)} - \delta_{\mathrm{T\_Rect}(w',h')}. \tag{8}$$

Here, $\delta_{\mathrm{R\_Rect}(w,h)}$ and $\delta_{\mathrm{T\_Rect}(w,h)}$ represent the light loss in R and T measurements, respectively. "Rect(w,h)" in the subscript denotes the rectangular incident light, whose (width, height) was (w cm, h cm).

3 Results

3.1 Distribution of reflectance and transmittance with various incident light beams

In the R and T distribution simulations, two pairs of optical properties were set based on two typical tissues, normal fatty tissue in breast *in vitro* (μ_a is 0.08 cm^{-1}, μ_s is 7.67 cm^{-1} at 789 nm) and Caucasian female skin *in vitro* (μ_a is 0.97 cm^{-1}, μ_s is 27.3 cm^{-1} at 810 nm, here the g was assumed as 0.7) [24]. Both in Figs. 3 and 4, the upper panel has a lower scattering property, and the incident light beams from left subfigure to right were rectangular, circular, and pencil, respectively. The (width, height) of the rectangular beam was (0.5 cm, 1.3 cm) and (0.7 cm, 1.6 cm) for R and T measurement, respectively; the radius of the circular beam was 0.45 and 0.60 cm for R and T measurement, respectively. In these two figures, the color indicates the $\log_{10}$ value of the response, R or T. The dark blue and the dark red represent the lowest and the highest intensity of the responses, respectively. The black enclosed curves denote the light incident ports for R and T measurements,

Table 1 Optical properties and thicknesses for modeling R and T

No.	name of layer	μ_a/cm^{-1}	μ_s/cm^{-1}	g	n	thickness/cm
1	glass	0	0	0	1.515	0.1
2	sample	0.0002 – 100	1 – 1000	0.7	1.37	0.11
3	glass	0	0	0	1.515	0.1

Notes: μ_a–absorption coefficient; μ_s–scattering coefficient; g–anisotropy; n–refractive index

which has mentioned in the subsection 2.1.

Figure 3 shows the distributions of R with various incident light beams. The most reflected light was concentrated on the incident area, and the escaped light caused by rectangular, circular and pencil incident light beams was respectively 26.54%, 25.19% and 23.74% (see Figs. 3(a)–3(c)). The distribution of R was much more even in the upper panel, which denotes a higher light loss. For example, with a rectangular beam incident, the light loss with higher μ_a and μ_s (Fig. 3(d)) was 4.62%, while that with lower μ_a and μ_s (Fig. 3(a)) was 26.54% (about 6 times of 4.62%).

Figure 4 shows a similar result in T measurement like Fig. 3. In the sequence of rectangular, circular and pencil incident light beams, the light loss decreased from 6.39% to 4.77% in the upper panel, and from 4.20% to 1.74% in the lower panel. Much light was escaped from detection area in the upper panel, such as, 6.39% light was lost in Fig. 4(a) which was larger than 4.20% in Fig. 4(d), and whereas the absolute difference of the light loss between the upper and the lower panel was larger in the R measurement (Fig. 3) than that in the T measurement (Fig. 4).

3.2 Effect of light beam shape on measurements of R and T

To study the effect of light beams on light losses, three kinds of incident light beams (rectangular, circular, pencil) were chosen in the R and T modeling. The results of the light loss and the absolute difference between rectangular incident light beam and other two incident light beams are shown in Figs. 5 and 6, respectively.

Figure 5 shows the light loss in the R (the upper panel) and T (the lower panel) with rectangular, circular and pencil incident light beam, and with various optical properties of turbid media. The upper panel shows that the light loss in the R measurement was decreased in the sequence of rectangular, circular and pencil incident light beam, and a similar result appeared in the T measurement (lower panel). In the R measurement, the light loss was increased fast to a peak value at μ_s of 4.0 cm^{-1} (such as 32% with rectangular incident beam where μ_a is 0.07 cm^{-1}) and then decreased significantly to a low value below 4% with the increase of μ_s, where the range of μ_a is 0.07 to 3.76 cm^{-1}; when μ_a is larger than 7.25 cm^{-1}, the light loss was very low (below 1%). In the T measurement, the light loss was increased fast to a peak value and then decreased slightly when μ_a is 0.07 cm^{-1}; at μ_a of 1.95 cm^{-1}, the light loss was increased slightly without decreased; when μ_a is larger than 7.25 cm^{-1}, the light loss was below 2%.

Figure 6 shows the absolute differences of the light loss with the rectangular incident light beam and the other light beams, circular and pencil. From Fig. 6, it can be found that the light loss with rectangular incident light beam was 0.2%–1.7% larger than that with circular incident beam, and about 0.5%–3.3% larger than that with pencil incident

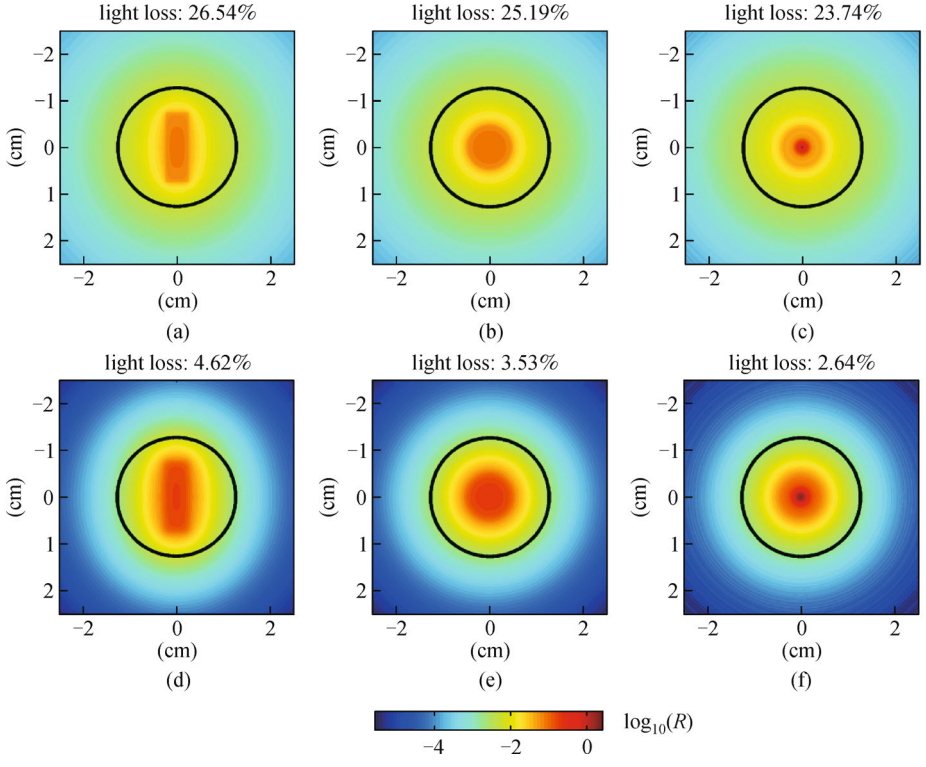

Fig. 3 Distribution of reflectance with various incident light beams: rectangular, circular and pencil light beams (from left to right). The optical properties of upper panel and the lower panel are (μ_a: 0.08 cm^{-1}, μ_s: 7.67 cm^{-1}) and (μ_a: 0.97 cm^{-1}, μ_s: 27.3 cm^{-1}), respectively. The light loss for each is also presented

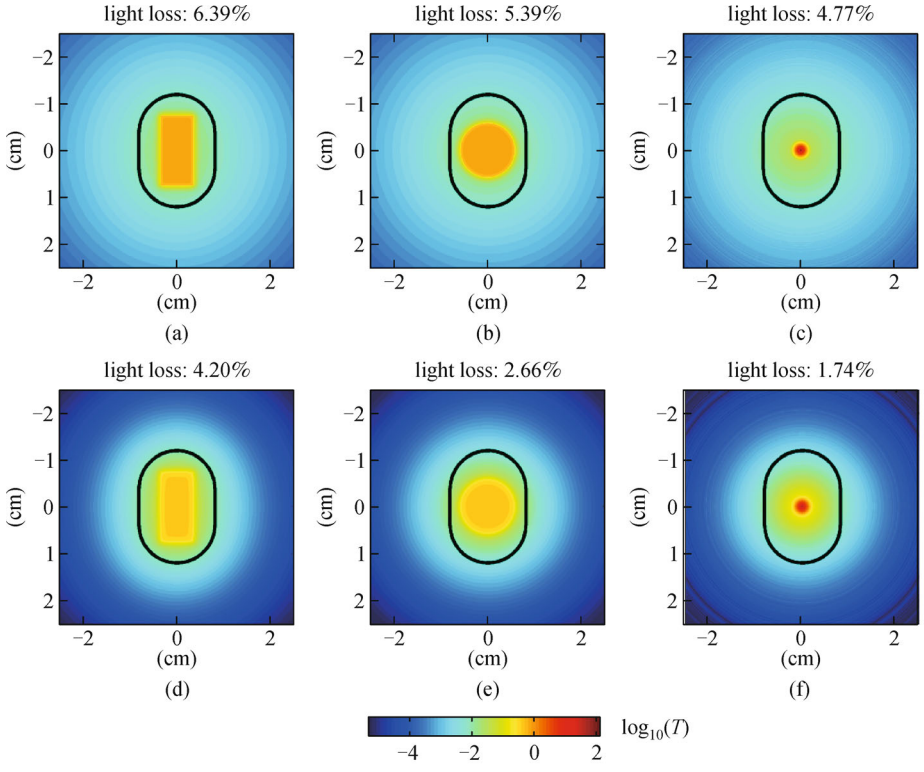

Fig. 4 Distribution of transmittance with various incident light beam, rectangular, circular and pencil light beam (from left to right). The optical properties of upper panel and the lower panel are (μ_a: 0.08 cm^{-1}, μ_s: 7.67 cm^{-1}) and (μ_a: 0.97 cm^{-1}, μ_s: 27.3 cm^{-1}) respectively, and the light loss for each is presented

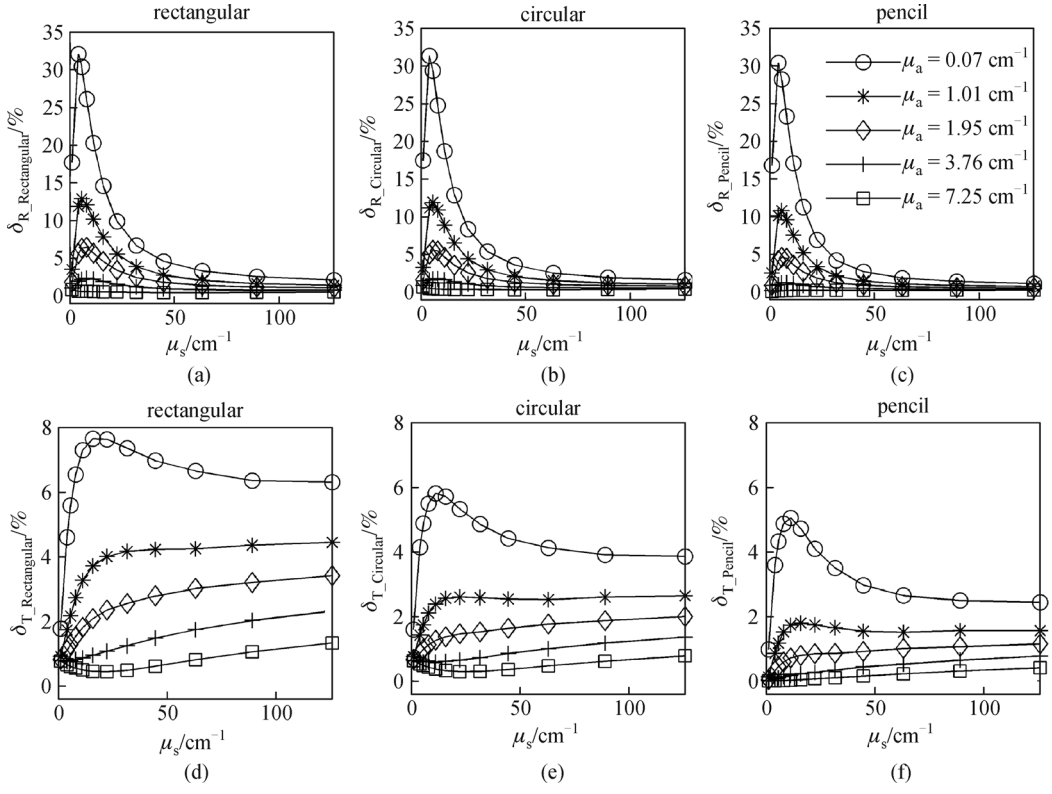

Fig. 5 Light losses in the *R* and *T* measurement with various incident light beam (rectangular, circular and pencil beam) and various optical properties of turbid media

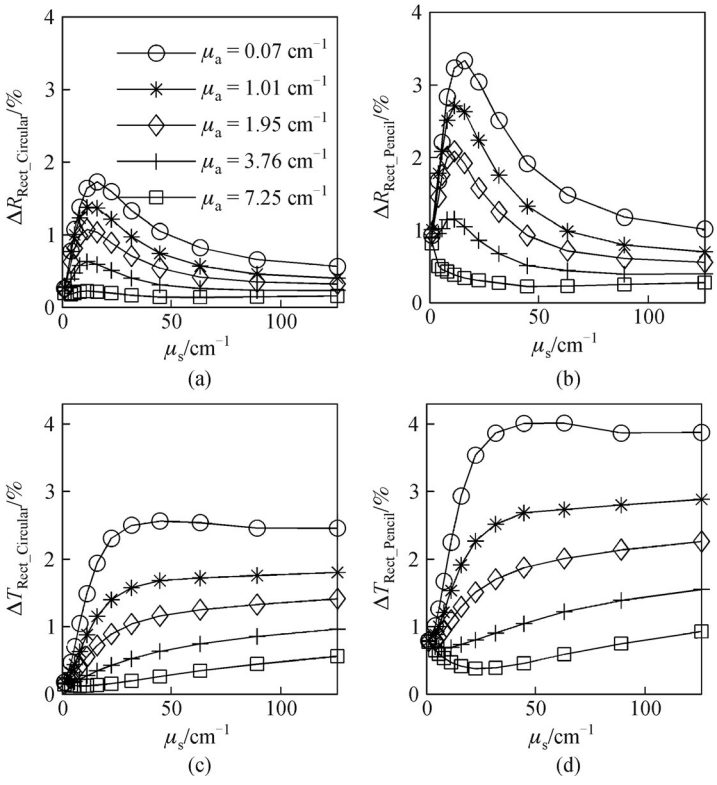

Fig. 6 Absolute differences of the light loss with the rectangular incident light beam and the other light beams, circular and pencil. The upper panel is the value in the *R* measurement, and the lower panel is in the *T* measurement

light in the *R* measurement when μ_a was below 1.95 cm^{-1}; when μ_a was larger than 3.76 cm^{-1}, the absolute difference with various incident light was very low ($<0.63\%$ between rectangular and circular, $<1.2\%$ between rectangular and pencil). In the *T* measurement, the difference of the light loss between the rectangular and the circular incident light was 0.14%–2.6%, and that was 0.77%–4.0% between the rectangular and the pencil incident light when μ_a was below 1.95 cm^{-1}; when μ_a was larger than 3.76 cm^{-1}, the absolute error was below 1% between rectangular and circular incident light beam, and was below 1.5% between rectangular and pencil incident light beam. No matter in the *R* or *T* measurement, all of the absolute differences was decreased with the increase of μ_a.

3.3 Effect of rectangular light beam size on measurement of *R* and *T*

To control the size of the incident light, the slit in the Lambda 950 was set as 2 nm, and the common beam mask was set as 60% at first, which made the (width, height) pair at *R* and *T* entrance as (0.5 cm, 1.3 cm) and (0.7 cm, 1.6 cm), respectively. Then, the slit and the common beam mask were set as 1 nm and 20% to make the (width, height) reduce to (0.4 cm, 0.8 cm) and (0.7 cm, 1.4 cm) at *R* and *T* entrance, respectively.

Based on the above various incident light size, the light loss was simulated, and the difference of the light loss in the *R* and *T* measurement with different size of rectangular incident light beam was given in Fig. 7. The difference of the light loss was 0.25%–1.40% in the *R* measurement when $\mu_a \leqslant 1.95$ cm^{-1} and $\mu_s \geqslant 4$ cm^{-1}, and when $\mu_a \geqslant 3.76$ cm^{-1}, the difference was below 0.5%; in the *T* measurement, the difference was all below 0.6%, because the size of the incident light in the *T* measurement was not dramatically changed by Lambda 950.

4 Discussion

The simulated distributions of the *R* and *T* with various light beams incident on the two typical samples had been given to show the light loss in a direct way. Then, the light losses with various incident light shapes and size, and various optical properties were compared.

With various incident light beam, the light loss was decreased in the sequence of rectangular, circular and pencil light beams. When μ_a was larger than 7.25 cm^{-1}, the absolute difference between various incident light beams was not significant, particularly between the rectangular and circular incident light beam in the *R* measurement (below 0.2%). In this condition, the light losses in all

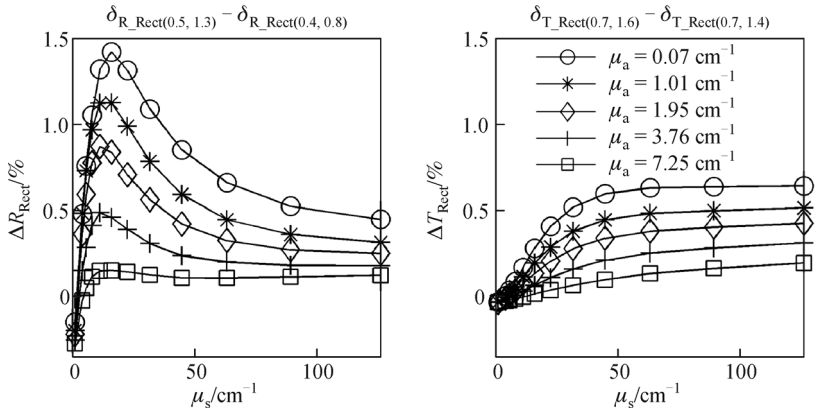

Fig. 7 Absolute differences of the light loss in *R* and *T* measurement with various size of the rectangular incident light beam

incident light beams were also very low. Thus, for a media which has a high absorption property, both the light loss in the *R* and *T* measurement, and the difference with various incident light beam, can be neglected. However, in the measurement of the biologic media, this condition usually could not be met, because the absorption properties of most biologic samples are lower than 7.25 cm^{-1}, such as, normal fatty tissue in breast (μ_a is 0.08 cm^{-1} at 789 nm), Caucasian female skin (μ_a is 0.97 cm^{-1} at 810 nm), liver tissue (μ_a is 2.3 cm^{-1} at 635 nm) and dermis in skin (μ_a is 2.7 at 700 nm) [24]. When μ_a was 1.95 cm^{-1}, the highest absolute differences between rectangular and circular beams were 1.1% in the *R* measurement and 1.4% in the *T* measurement; the highest differences between rectangular and pencil were 2.0% and 2.2%, respectively. Although, the absolute value here was not high, it also should be paid attention to in calculating optical properties with the measurement results, because perturbing the *R* and *T* values by 1% would result in errors of 17% for μ_a [25]. The decrease of the incident light size also can reduce the light loss, but this will weaken the intensity of the incident light, and may influence the accuracy in the measurement.

The effect of the optical properties on the light loss was also discussed in detail. The light loss was decreased with the increase of μ_a, which was in coincidence with the work in Ref. [16]. While a lot of biologic tissues have a low μ_a, the light loss should not be neglected directly in the measurement. The second optical property, μ_s, must be considered together. With the increase of μ_s, the light loss was increased to a peak value (μ_s = 4 cm^{-1}) and then decreased to a value below 2% ($\mu_s > 100$ cm^{-1}); in the *T* measurement, the light loss was increased first and then decreased slightly ($\mu_a < 0.07$ cm^{-1}) or increased without decreased ($1.01 < \mu_a < 1.95$ cm^{-1}), and with a low μ_a, such as 0.07 cm^{-1}, the light loss would be 6.3% ($\mu_s > 100$ cm^{-1}, rectangular beam incident) which was larger than that, 2.6%, in the *R* measurement. Thus, in the measurement of the sample which has low optical properties, μ_a (close to 0 cm^{-1}) and μ_s (close to 2 cm^{-1}), the light loss would be large. In measuring the *R* of the normal fatty tissue in breast (μ_a is 0.08 cm^{-1} and μ_s is 7.67 cm^{-1} at 789 nm) with rectangular light beam incident, the light loss would be about 26%, and 4.6% for Caucasian female skin (μ_a is 0.97 cm^{-1} and μ_s is 27.3 cm^{-1} at 810 nm), < 1.4% for liver tissue (μ_a is 2.3 cm^{-1} and μ_s is 313 cm^{-1} at 635 nm) [24]; in the *T* measurement of the normal fatty tissue in breast, the Caucasian female skin and liver tissue, the losses were about 7.9%, 4.0% and 3.0%, respectively.

In conclusion, to measure the *R* or *T* much more accurately, the optical properties of the sample should be considered before the light shape and size according to their effect on light loss. If the sample has a high μ_a (> 7.25 cm^{-1}), the light loss in the *R* and *T* measurement can be neglected; if μ_a of sample is below 7.25 cm^{-1} and μ_s is above 100 cm^{-1}, the light loss also can be neglected in the *R* and *T* measurement. When μ_a and μ_s are in the other range, the light loss can be decreased using other method, such as increasing the size of the integrating sphere port, or reducing the size of the light beams close to the pencil beam.

5 Conclusions

This work implemented the convolution for obtaining the response to the rectangular incident light beam, and then investigated the effect of light beam shape and size, and optical properties of sample on *R* and *T* measurements with integrating sphere. The results show that the light loss with various incident light beam is in the following sequence, rectangular > circular > pencil. The light loss induced by the optical properties of sample is much more significant than that by the shape and size of the incident light beam. This study can be helpful for choosing a suitable incident light to measure the *R* and *T* of a particular turbid sample and predicting the measuring error.

Acknowledgements This study was supported by the National Natural Science Foundation of China (Grant Nos. 81171376 and 91232710), the Research Fund for the Doctoral Program of Higher Education of China (No. 20110142110073), and the Science Fund for Creative Research Group of China (No. 6141064).

References

1. Noda H M, Motohka T, Murakami K, Muraoka H, Nasahara K N. Accurate measurement of optical properties of narrow leaves and conifer needles with a typical integrating sphere and spectro-radiometer. Plant, Cell & Environment, 2013, 36(10): 1903–1909
2. van Staveren H J, Moes C J M, van Marie J, Prahl S A, van Gemert M J C. Light scattering in Intralipid-10% in the wavelength range of 400 – 1100 nm. Applied Optics, 1991, 30(31): 4507–4514
3. Aernouts B, Zamora-Rojas E, Van Beers R, Watté R, Wang L, Tsuta M, Lammertyn J, Saeys W. Supercontinuum laser based optical characterization of Intralipid® phantoms in the 500 – 2250 nm range. Optics Express, 2013, 21(26): 32450–32467
4. Zamora-Rojas E, Aernouts B, Garrido-Varo A, Saeys W, Perez-Marin D, Guerrero-Ginel J E. Optical properties of pig skin epidermis and dermis estimated with double integrating spheres measurements. Innovative Food Science & Emerging Technologies, 2013, 20: 343–349
5. Zhong X, Wen X, Zhu D. Lookup-table-based inverse model for human skin reflectance spectroscopy: two-layered Monte Carlo simulations and experiments. Optics Express, 2014, 22(2): 1852–1864
6. Kim S, Jeong S. Effects of temperature-dependent optical properties on the fluence rate and temperature of biological tissue during low-level laser therapy. Lasers in Medical Science, 2014, 29(2): 637–644
7. Välisuo P, Kaartinen I, Tuchin V, Alander J. New closed-form approximation for skin chromophore mapping. Journal of Biomedical Optics, 2011, 16(4): 046012
8. Adams M T, Wang Q, Cleveland R O, Roy R A. Thermal dose dependent optical property changes of ex vivo chicken breast tissues between 500 and 1100 nm. Physics in Medicine and Biology, 2014, 59(13): 3249–3260
9. Bashkatov A N, Genina E A, Kochubey V I, Gavrilova A A, Kapralov S V, Grishaev V A, Tuchin V V. Optical properties of human stomach mucosa in the spectral range from 400 to 2000 nm: prognosis for gastroenterology. Medical Laser Application, 2007, 22 (2): 95–104
10. Bashkatov A N, Genina E A, Kochubey V I, Rubtsov V S, Kolesnikova E A, Tuchin V V. Optical properties of human colon tissues in the 350 – 2500 nm spectral range. Quantum Electronics, 2014, 44(8): 779–784
11. Bosschaart N, Edelman G J, Aalders M C, van Leeuwen T G, Faber D J. A literature review and novel theoretical approach on the optical properties of whole blood. Lasers in Medical Science, 2014, 29(2): 453–479
12. Grabtchak S, Montgomery L G, Whelan W M. Optical absorption and scattering properties of bulk porcine muscle phantoms from interstitial radiance measurements in 650-900 nm range. Physics in Medicine and Biology, 2014, 59(10): 2431–2444
13. Zamora-Rojas E, Aernouts B, Garrido-Varo A, Perez-Marin D, Guerrero-Ginel J, Saeys W. Double integrating sphere measurements for estimating optical properties of pig subcutaneous adipose tissue. Innovative Food Science & Emerging Technologies, 2013, 19(0): 218–226
14. Zhang L, Shi A, Lu H. Determination of optical coefficients of biological tissue from a single integrating-sphere. Journal of Modern Optics, 2012, 59(2): 121–125
15. Zhang Y, Chen Y, Yu Y, Xue X, Tuchin V V, Zhu D. Visible and near-infrared spectroscopy for distinguishing malignant tumor tissue from benign tumor and normal breast tissues *in vitro*. Journal of Biomedical Optics, 2013, 18(7): 077003
16. Zhu D, Lu W, Zeng S, Luo Q. Effect of light losses of sample between two integrating spheres on optical properties estimation. Journal of Biomedical Optics, 2007, 12(6): 064004
17. Pickering J W, Prahl S A, van Wieringen N, Beek J F, Sterenborg H J C M, van Gemert M J C. Double-integrating-sphere system for measuring the optical properties of tissue. Applied Optics, 1993, 32 (4): 399–410
18. Friebel M, Helfmann J, Meinke M C. Influence of osmolarity on the optical properties of human erythrocytes. Journal of Biomedical Optics, 2010, 15(5): 055005
19. Morawiec S, Mendes M J, Filonovich S A, Mateus T, Mirabella S, Aguas H, Ferreira I, Simone F, Fortunato E, Martins R, Priolo F, Crupi I. Broadband photocurrent enhancement in a-Si:H solar cells with plasmonic back reflectors. Optics Express, 2014, 22(S4 Suppl 4): A1059–A1070
20. Bruns S, Rademacher D, Vergöhl M, Weiss P. Properties of reactive sputtered alumina-silica mixtures. Applied Optics, 2014, 53(4): A334–A338
21. Cong A X, Hofmann M C, Cong W, Xu Y, Wang G. Monte Carlo fluorescence microtomography. Journal of Biomedical Optics, 2011, 16(7): 070501
22. Wang L, Jacques S L, Zheng L. MCML—Monte Carlo modeling of light transport in multi-layered tissues. Computer Methods and Programs in Biomedicine, 1995, 47(2): 131–146
23. Wang L, Jacques S L, Zheng L. CONV—convolution for responses to a finite diameter photon beam incident on multi-layered tissues. Computer Methods and Programs in Biomedicine, 1997, 54(3): 141–150
24. Vo-Dinh T. Biomedical Photonics Handbook. New York: CRC Press, 2003
25. Prahl S A, van Gemert M J C, Welch A J. Determining the optical properties of turbid mediaby using the adding-doubling method. Applied Optics, 1993, 32(4): 559–568

Xiewei Zhong recevied the B.S. degree in biomedical engineering from Huazhong University of Science and Technology (HUST), Wuhan, China, in 2012. He is currently working toward the M.S. degree in biomedical engeerning from HUST. His research interests include reflectance spectroscopy and tissue optical-property measurement.

Shenxia Tan studied biomedical engineering at the Southern Medical University in Guangzhou, China, where she received her bachelor's degree in 2010. From 2010 to 2013, she, as a graduate student, worked on tissue optical-property measurement with an integrating sphere based on Monte Carlo simulation in the group of Prof. Dan Zhu at the Britton Chance Center for Biomedical Photonics, Wuhan National Laboratory for Optoelectronics, Huazhong University of Science and Technology, Wuhan, China. And in 2013, she received her master degree and now works as a software tester in Huawei Technology Co., Ltd.

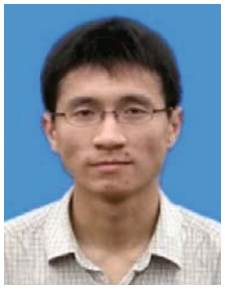

Xiang Wen studied biomedical engineering at Huazhong University of Science and Technology (HUST), Wuhan, China, Where he received his bachelor's degree in 2007 and Ph.D. degree in 2012. During his doctoral thesis, he worked on mechanisms of skin optical clearing and optical properties measurement of skin tissue in the group of Prof. Dan Zhu at the Britton Chance Center for Biomedical Photonics, Wuhan National Laboratory for Optoelectronics, HUST. He is now an employee of Shanghai Siemens Medical Equipment Ltd.

Dan Zhu received the B.S. degree in physics from Hubei University, in 1986, the M.S. degree in radioelectronics from Central China Normal University, in 1992, and the Ph.D. degree in physical electronics from Huazhong University of Science and Technology (HUST), in 2001. After having completed a Postdoctoral Fellowship in biomedical engineering at HUST, she got the position of Associate Professor in biomedical engineering in 2003, and Full Professor in 2007. She is currently as a Professor of Wuhan National Optoelectronics Laboratory, HUST. She has authored more than 100 papers in the field of tissue optics, optical diagnosis, and therapy principle and techniques. During the recent years, she has been focusing on optical clearing of tissue *in vivo*. She is also the Secretary General of Biomedical Photonics Committee of Chinese Optical Society.